JOURNAL OF MATERIALS SCIENCE 32 (1997) 957–964

Effect of interlayer anions on the physicochemical properties of zinc–aluminium hydrotalcite-like compounds

S. VELU, V. RAMKUMAR, A. NARAYANAN and C. S. SWAMY*
Department of Chemistry, Indian Institute of Technology, Madras 600036, India

Zinc–aluminium hydrotalcite-like compounds (ZnAlA^{n-}–HT) with a Zn/Al atomic ratio 2.0 and $A^{n-} = CO_3^{2-}$, Cl^-, NO_3^- and SO_4^{2-}, were synthesized by coprecipitation under low supersaturation. Their physicochemical properties were studied using powder X-ray diffraction (PXRD), infrared (IR) and laser Raman (LR) spectra, thermogravimetry (TG), differential scanning calorimetry (DSC), evolved gas analysis (EGA), ^{27}Al MAS NMR, BET surface area and pore-size determination. The PXRD of the synthesized samples showed that the crystallinity was affected by the nature of the anions present in the interlayer space. The IR and LR studies revealed that except the NO_3^- ion, the symmetry of these interlayer anions was reduced upon intercalation. The TG, DSC and EGA results showed two or three stages of weight loss corresponding to the removal of the interlayer water, structural water and the anion, respectively. The activation energy, E_a, for the decomposition process was found to decrease in the order ZnAlCO_3–HT > ZnAlSO_4–HT > ZnAlCl–HT > ZnAlNO_3–HT. Formation of a pentacoordinated Al (Al^V) in addition to the octahedral (Al^{VI}) and tetrahedral Al (Al^{IV}) was the special feature noticed in the ^{27}Al MAS NMR of the calcined samples. Thermal calcination around 500 °C resulted in the formation of non-stoichiometric ZnO whose crystallinity decreased in the order ZnAlNO_3–CHT > ZnAlCl–CHT > ZnAlSO_4–CHT > ZnAlCO_3–HT while their extent of solid solubility was found to be the reverse. The crystallinity of the calcined samples was also correlated with surface area and pore-size determination.

1. Introduction

Hydrotalcites (HT) are composed of positively charged brucite-like layers of divalent and trivalent metal hydroxides whose excess positive charge is compensated by anions and water molecules present in the interstitial position. They can be represented by the general formula $[M(II)_{1-x}M(III)_x(OH)_2]^{x+}[A^{n-}_{x/n} \cdot YH_2O]^{x-}$, where M(II) = Mg, Ni, Co, Cu, Zn, Mn; M(III) = Al, Fe, Cr, V; $A^{n-} = CO_3^{2-}$, Cl^-, SO_4^{2-}, etc., and $x = 0.1$–0.35. Numerous studies on the synthesis and physicochemical properties of CO_3^{2-} interlayered HT have been reported owing to their potential use as precursors for the synthesis of well-dispersed, mixed oxides which are mainly used as base catalysts [1–8]. Synthesis of HT with Cl^- and NO_3^- as interlayer anions have received considerable attention in recent years because of their large anion-exchanging capacity. Ookubo *et al.* [9] have synthesized PO_4^{3-} intercalated HT using MgAlCl–HT and ZnAlCl–HT as precursors with an endeavour to use them as phosphate binders for controlling hyperphosphatemia. Mousty *et al.* [10] exchanged the Cl^- ion in ZnCr–HT by electroactive organic anions and used them as clay-modified electrodes. The NO_3^- interlayered HT was used as a precursor for pillaring of robust polyoxometallates [11]. Recently, Constantino and Pinnavaia [12] have reported that the nature of the interlayer anions plays a crucial role in controlling the catalytic activity. However, reports available on the effect of various interlayer anions on the physicochemical properties of zinc–aluminium hydrotalcite-like compounds are scarce [13, 14]. The aim of the present investigation was to study the effect of CO_3^{2-}, Cl^-, NO_3^- and SO_4^{2-} as interlayer anions on the physicochemical properties of zinc–aluminium HT having the approximate stoichiometric formula, $Zn_4Al_2(OH)_{14}A^{n-} \cdot YH_2O$. In the following sections, these compounds will be represented as ZnAlCO_3–HT, ZnAlCl–HT, ZnAlNO_3–HT and ZnAlSO_4–HT, respectively.

2. Experimental procedure

2.1. Materials

Zinc–aluminium HT with a Zn/Al atomic ratio around 2, containing NO_3^-, Cl^-, SO_4^{2-} and CO_3^{2-} as interlayer anions, were synthesized at room temperature by the coprecipitation method under low supersaturation conditions [2, 15], maintaining a nitrogen atmosphere. A mixture of 1M solutions of $Zn(NO_3)_2$ or $ZnSO_4$ and $Al(NO_3)_3$ or $AlCl_3$ as precursor and a 2M solution of NaOH as precipitant were used. The

0022–2461

resultant slurry was aged at 65 °C for 30 min, filtered, washed with deionized water until the pH of the filtrate was 7, and dried at 100 °C for 12 h.

2.2. Techniques

The experimental details for elemental analysis (ICPES), differential scanning calorimetry (DSC), evolved gas analysis (EGA) and ^{27}Al MAS NMR are given elsewhere [15, 16]. The powder X-ray diffraction (PXRD) patterns of the samples were recorded in a Rigaku instrument using nickel-filtered CuK_α radiation ($\lambda = 0.15408$ nm) for qualitative purpose. For the calculation of lattice parameters and particle size a Phillips X-ray generator (Model PW 1130) using iron-filtered CoK_α radiation ($\lambda = 0.179\,02$ nm) at a scan speed of $2\theta = 1^\circ\,\text{min}^{-1}$ was used. The 2θ values were corrected using silicon as an external standard. IR spectra were recorded in a Shimadzu 470 instrument employing KBr pellet technique. Laser Raman spectra of all these samples were recorded with a Z24 Dilor Raman microprobe. With this instrument, a spectra Physics model 165 argon laser served as the photon source and the spectra were typically obtained by the use of the 488 nm excitation line. Thermogravimetry (TG) of the compounds was recorded in a Perkin–Elmer TG/DSC-7 in the temperature range 50–900 °C at a scan speed of 5, 10 and 20 °C min^{-1} under a nitrogen atmosphere. The activation energy, E_a, for the decomposition process was calculated using kinetic software, applying the Arrhenius equation. The surface area and pore-size determinations were carried out employing the BET N_2 adsorption–desorption method at 77 K using a Carlo Erba (Model 1800) sorptometer. Prior to the adsorption of nitrogen gas, the samples were out-gased in an evacuation chamber (Carlo Erba out-gassing unit with Pirani gauge) to a pressure of 10^{-3} atm, at 120 °C.

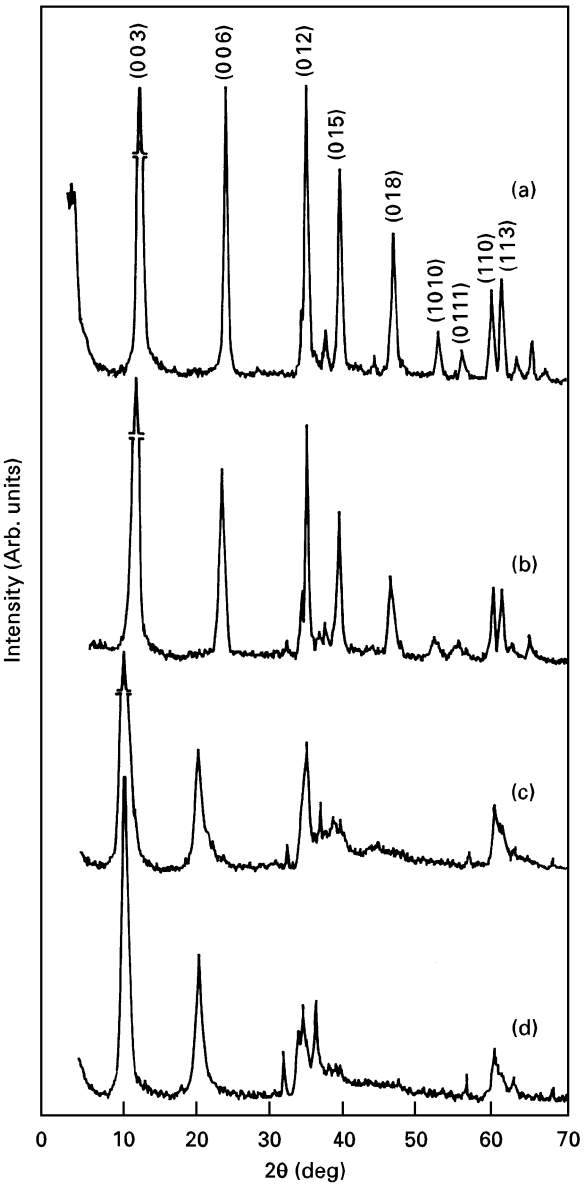

Figure 1 Powder X-ray diffraction patterns of (a) $ZnAlCO_3$–HT, (b) ZnAlCl–HT, (c) $ZnAlNO_3$–HT, (d) $ZnAlSO_4$–HT.

3. Results and discussion

Table I summarizes the chemical composition derived from the results of inductively coupled plasma emission spectroscopy (ICPES), TG, DSC and EGA. The anion content (Cl^-, NO_3^- and SO_4^-) have been estimated employing a volumetric titration technique as reported by Hernandez *et al.* [13]. The PXRD of these samples (Fig. 1) exhibited sharp and symmetric peaks at low 2θ angles and broad and asymmetric peaks at higher 2θ angles which are characteristic of clay minerals possessing a layered structure and they are very similar to the pattern of natural hydrotalcite [17]. However, the intensity of all the peaks [(0 0 3), (0 0 6), (0 1 2), (0 1 8), (1 1 0) and (1 1 3)] decreased in the order $ZnAlCO_3$–HT > ZnAlCl–HT > $ZnAlNO_3$ – HT > $ZnAlSO_4$–HT which indicates a decrease in

TABLE I Chemical composition and poweder X-ray diffraction data for ZnAlA^{n-}-HT

Sample	Zn/Al[a] atomic ratio	Sample formula	Lattice parameter[b]			Average crystal size[c]
			a_0 (nm)	c_0 (nm)	V (10^{-3} nm^3)	(nm)
$ZnAlCO_3$–HT	1.8	$Zn_{0.64}Al_{0.36}(OH)_2(CO_3)_{0.18}\cdot 0.86H_2O$	0.3061	2.2414	181.88	25.24
ZnAlCl–HT	1.8	$Zn_{0.64}Al_{0.36}(OH)_2(Cl)_{0.28}(CO_3)_{0.03}\cdot 0.55H_2O$	0.3073	2.3053	188.53	20.05
$ZnAlNO_3$–HT	1.7	$Zn_{0.63}Al_{0.37}(OH)_2(NO_3)_{0.30}(CO_3)_{0.04}\cdot 0.52H_2O$	0.3056	3.2241	260.76	17.97
$ZnAlSO_4$–HT	1.9	$Zn_{0.66}Al_{0.34}(OH)_2(SO_4)_{0.06}(CO_3)_{0.03}\cdot 0.87H_2O$	0.3062	3.2640	265.03	15.16

[a] Determined from ICPES, TGA, EGA and volumetric analysis [13].
[b] Calculated employing the least square fitting method for a hexagonal crystal system.
[c] Calculated from X-ray line broadening (at higher 2θ angles).

TABLE II Basal spacings and gallery heights of ZnAlA^{n-}—HT

Compound	Basal spacing $d_{(0\,0\,3)}$ (nm)	Anion diameter (nm)	Gallery height (nm)
$ZnAlCO_3$–HT	0.7379	0.370	0.2609
ZnAlCl–HT	0.7639	0.362	0.2869
$ZnAlNO_3$–HT	0.8533	0.378	0.3763
$ZnAlSO_4$–HT	0.8584	0.472	0.3814

crystallinity upon intercalation with anions other than CO_3^{2-}. The observed trend in the crystallinity is also corroborated by the decrease in average particle size from 25.24 nm for $ZnAlCO_3$–HT to 15.16 nm for $ZnAlSO_4$–HT (Table I). These results can be attributed to the degree of disturbance in the structure which is influenced by the anion diameter whose order is $SO_4^{2-} > NO_3^- > Cl^- \approx CO_3^{2-}$ (Table II). The PXRD pattern also showed that, in the case of $ZnAlNO_3$–HT and $ZnAlSO_4$–HT, the intensity of the (1 1 0) plane (assumed to be the cell dimension, a_0, of the brucite-like layer) decreased markedly and the peak corresponding to the (0 1 8) plane becomes almost absent. This may be due to the strong adsorption of Cl^-, NO_3^- and SO_4^{2-} ions on the positively charged layer compared to the CO_3^{2-} ion. The cell dimensions are calculated by indexing the peaks under the hexagonal crystal system, applying the method of least square fittings [15, 16] (Table I). The a_0 values remain almost constant for all the compounds, irrespective of the interlayer anions. However, the c_0, values depend both on the size and the charge of the anion. The gallery height was calculated by subtracting the thickness of the brucite-like layer [18] (0.477 nm) from the thickness of the unit layer ($d_{(0\,0\,3)}$ basal spacing) (Table II). The gallery height increases with increase in anion diameter, with consequent increase in the c_0 value. The higher gallery height of ZnAlCl–HT (0.2869 nm) compared to $ZnAlCO_3$–HT (0.2609 nm) demonstrates that the binding strength of the divalent anion with a basic layer is more than that of the monovalent anion. The gallery heights of $ZnAlCO_3$–HT, ZnAlCl–HT and $ZnAlSO_4$–HT are lower than the corresponding free anion diameter which implies the strong interaction of these anions with the brucite-like layer. The exceptionally higher gallery height (0.3763 nm) which is approximately equal to the diameter of the NO_3^- ion (0.378 nm) in the case of $ZnAlNO_3$–HT could be attributed to the vertical alignment of NO_3^- planar groups with respect to the host layer [19].

3.1. IR and laser Raman spectra

The IR and laser Raman (LR) studies were carried out in order to analyse the nature of the coordination/symmetry of the anion in the interlayer. If the symmetry of CO_3^{2-} (D_{3h}), NO_3^- (D_{3h}) and SO_4^{2-} (T_d) are retained in the interlayer, the IR inactive ν_1 bands would be expected to appear in LR. The IR spectrum of $ZnAlCO_3$–HT and $ZnAlNO_3$–HT showed (Fig. 2) sharp bands at 1357 and 1376 cm^{-1} which are

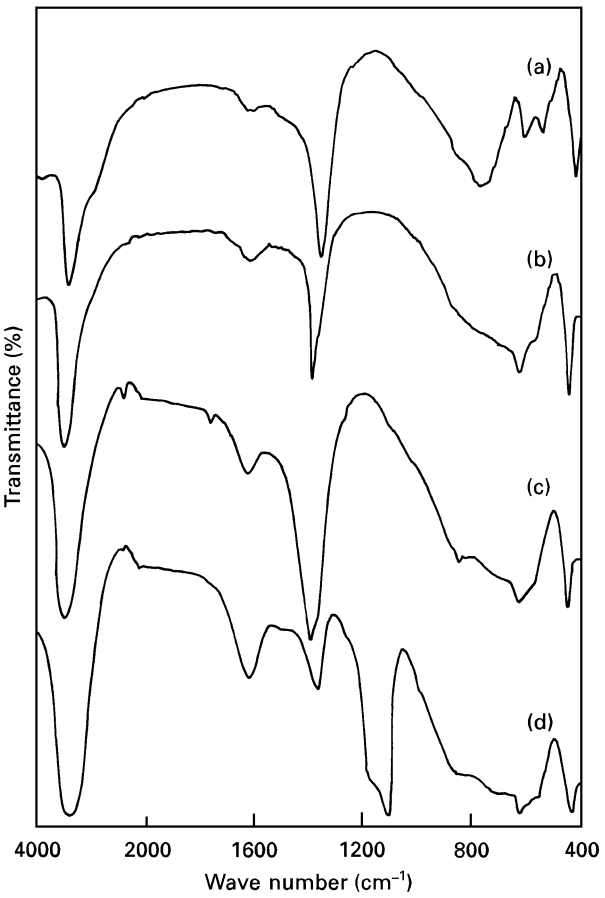

Figure 2 IR spectra of (a) $ZnAlCO_3$–HT, (b) ZnAlCl–HT, (c) $ZnAlNO_3$–HT, (d) $ZnAlSO_4$–HT.

attributed to the ν_3 vibrations of CO_3^{2-} and NO_3^- ions, respectively, indicating that the symmetry of these anions are not perturbed in the interlayer. However, the LR showed (Fig. 3) a strong and sharp band (1059 cm^{-1}) only in the case of $ZnAlNO_3$–HT while a weak band at 1081 cm^{-1} is noticed for $ZnAlCO_3$–HT. From these results it can be inferred that the NO_3^- ion in $ZnAlNO_3$–HT is present with very high symmetric environment while the CO_3^{2-} ion is perturbed at least to a small extent. The retention of the symmetry of NO_3^- ion in $ZnAlNO_3$–HT could be attributed to the vertical alignment of NO_3^- planar groups with respect to the host layer as evidenced from the PXRD data. In the case of $ZnAlSO_4$–HT, appearance of a weak band in IR at 982 cm^{-1} (ν_1) and splitting of the ν_3 vibration into 1104,1139 and 1181 cm^{-1}, are evidence for the perturbation of symmetry of SO_4^{2-} ion. The LR of $ZnAlSO_4$–HT is very diffuse, due to the fluorescence of the sample.

The $\nu_{H-O-H_{bent}}$ and $\nu_{OH_{sym}}$ bands in these compounds appear in the ranges 1610–1630 and 3440–3470 cm^{-1}, respectively. The lower values of $\nu_{OH_{sym}}$ in these compounds compared to that of free OH group (> 3650 cm^{-1}) indicates that all the OH groups are involved in hydrogen bonding with layer and interlayer. The most striking feature noticed here is the FWHM values of $\nu_{OH_{sym}}$ which are are calculated to be 275, 300, 450 and 575 cm^{-1} for $ZnAlCO_3$–HT, ZnAlCl–HT, $ZnAlNO_3$–HT and $ZnAlSO_4$–HT, respectively. The decrease in FWHM values in the order

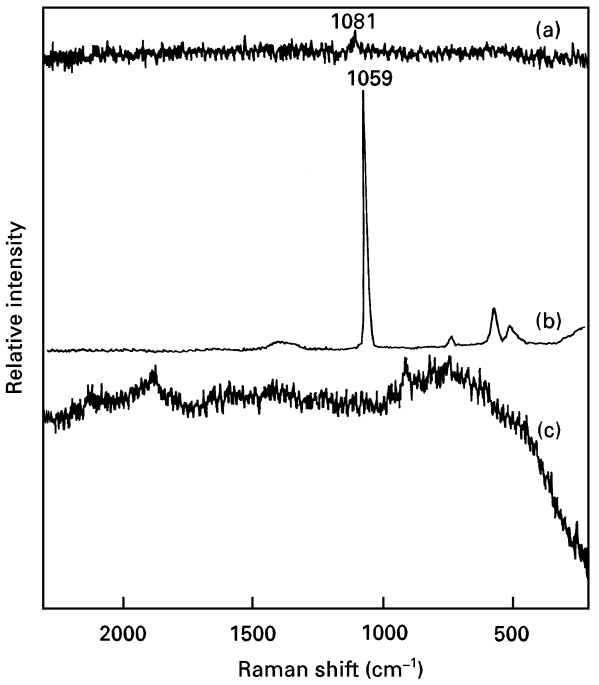

Figure 3 Laser Raman spectra of (a) $ZnAlCO_3$–HT, (b) $ZnAlNO_3$–HT, (c) $ZnAlSO_4$–HT.

$ZnAlCO_3$–HT > ZnAlCl–HT > $ZnAlNO_3$–HT > $ZnAlSO_4$–HT can be attributed to the decrease in cation distribution [20] in these samples.

3.2. Thermal characterization

Thermal properties of all the samples reported here have been studied by TG, DSC, EGA, PXRD ^{27}Al MAS NMR, surface area and pore-size determination. The TG/DTG plots of these samples are given in Fig. 4. In each case, the TG showed a first weight loss below 200 °C which is ascribed generally to the loss of physically adsorbed and interlayer water. The second weight loss in the temperature range 200–600 °C can be attributed to the decomposition of brucite-like layer and the removal of interlayer anions. In $ZnAlCO_3$–HT, the second weight loss appeared around 270 °C. The broad DTG peaks of ZnAlCl–HT reveals that the decomposition process is complex. It showed three weight loss processes below 300 °C which are ascribed to the loss of surface water and interlayer water. Two more stages of weight loss processes, one between 300 and 400 °C and the another between 450 and 600 °C are due to the removal of interlayer anions. The evolved gas analysis (EGA) of ZnAlCl–HT (Fig. 5) showed the evolution of CO_2, NO_2 and NO gases (deduced from their mass numbers) whose onset temperatures are around 130, 320 and 390 °C, respectively, and their maximum evolution was around 390 °C. The NO_2 and NO gases are evolved from the decomposition of the NO_3^- ion present in the interlayer together with the Cl^- ion. The weight loss between 450 and 600 °C in this compound can be attributed tentatively to the loss of HCl/Cl_2 gas from the decomposition of the Cl^- ions present in the interlayer. However, because the maximum furnace temperature attainable in the QMS instrument is

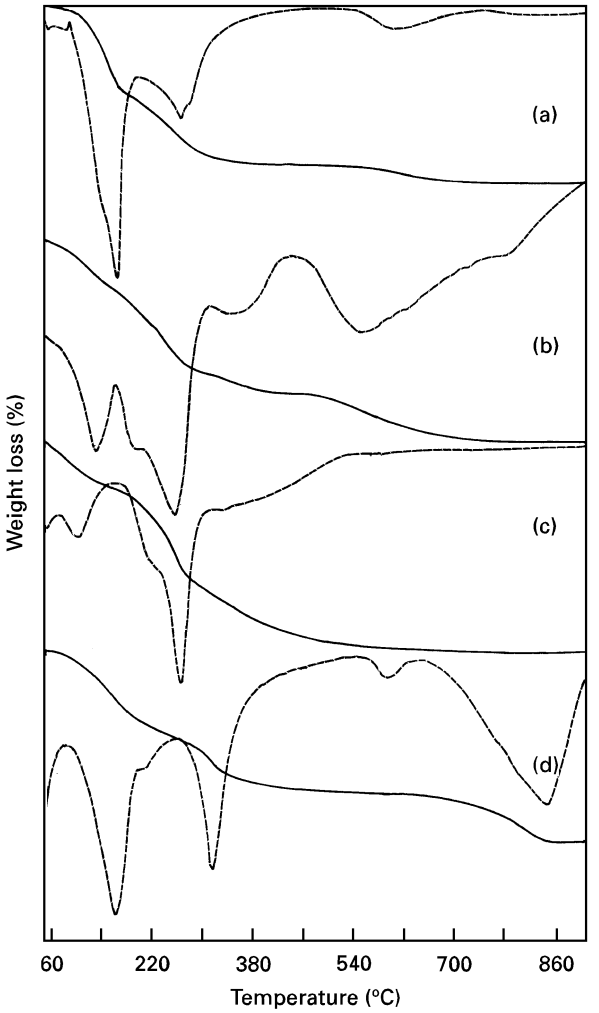

Figure 4 (——) TG and (· · ·) DTG traces of (a) $ZnAlCO_3$–HT, (b) ZnAlCl–HT, (c) $ZnAlNO_3$–HT, (d) $ZnAlSO_4$–HT.

400 °C, we could not record the evolution of these gases. Further experiments are in progress in order to verify this possibility. Similar to ZnAlCl–HT, $ZnAlNO_3$–HT also showed three stages of weight loss in TG suggesting the presence of different arrangements of water molecules in this sample as described earlier for ZnAlCl–HT. The EGA of $ZnAlNO_3$–HT showed the evolution of NO_2 and NO gases around 250 and 390 °C in two steps. The DTG of $ZnAlSO_4$–HT showed that the second weight loss occurs at 317 °C indicating a higher thermal stability of the compound. A third weight loss around 850 °C observed for this compound can be attributed to the complete decomposition of SO_4^{2-} in the interlayer into SO_3 gas [12]. The higher decomposition temperatures for ZnAlCl–HT and $ZnAlSO_4$–HT as compared to $ZnAlNO_3$–HT or $ZnAlCO_3$–HT are due to the non-vaporizable nature of the anions present in them.

The activation energy, E_a, for the decomposition process calculated from TG results is given in Table III. In the region 0%–15% decomposition, the majority of the loss is due to the removal of interlayer water along with a minimal loss of interlayer anion. Hence it may not be desirable to compare the E_a values in this region because it involves the difference in the amount of water and the strength of interaction

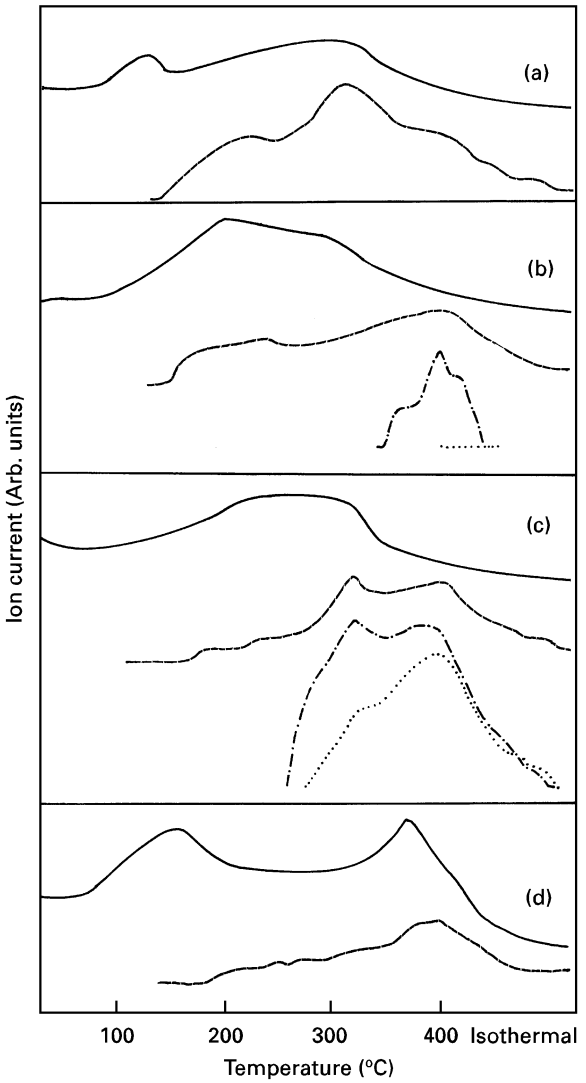

Figure 5 EGA traces of (a) $ZnAlCO_3$–HT, (b) ZnAlCl—HT, (c) $ZnAlNO_3$HT, (d) $ZnAlSO_4$–HT. (——) H_2O, (– – –) CO_2, (— · —) NO_2, (· · ·) NO.

between water and interlayer anions and/or brucite-like sheet. The E_a values at 20% weight loss, where the destruction of the brucite-like layer is maximum, clearly showed that the thermal stability of the layer is in the order $ZnAlCO_3$–HT > $ZnAlSO_4$–HT > ZnAlCl–HT > $ZnAlNO_3$–HT. The higher value of E_a for the divalent anion-HT compared to the monovalent anion-HT indicates the existence of a stronger binding force between the divalent anion and the basic layer (cf: PXRD results).

The evolution of CO_2 observed (by EGA) even in the case of ZnAlCl–HT, $ZnAlNO_3$–HT and $ZnAlSO_4$–HT, suggests that a small amount of CO_3^{2-} is always present in the interlayer, which is due to the inherent nature of these materials. The DSC results (Table IV) corroborate the TG results, giving two endothermic transformations corresponding to the two weight loss processes occurring in these samples.

The ^{27}Al MAS NMR spectra of all these compounds are shown in Fig. 6. The indicated chemical shifts are observed values without second-order quadrupole corrections using a 1M aqueous solution of $Al(NO_3)_3$ as reference. The ^{27}Al MAS NMR spectra of unheated samples generally shows a single resonance around 10 p.p.m. (Fig. 6a) indicating that all the aluminium is present in the octahedral coordination (Al^{VI}). Upon calcination, the development of a resonance around 70 p.p.m. is attributed to the aluminium present in the tetrahedral coordination (Al^{IV}). The most important observation is the appearance of a new resonance around 50 p.p.m. in the case of $ZnAlCO_3$–HT and $ZnAlSO_4$–HT. We ascribe this resonance to the pentacoordinated aluminium (Al^{V}). Indeed, we noticed a resonance corresponding to the Al^{V} in the temperature range 300–600 °C during the calcination of ZnAl 3.0–HT (unpublished results). This type of Al is reported to be present only in ρ-alumina which is formed during the thermal

TABLE III Activation energy, E_a, for the decomposition of $ZnAlA^{n-}$–HT (derived from TG)

	E_a (kJ mol^{-1})			
Decomposition (%)	$ZnAlCO_3$–HT	ZnAlCl–HT	$ZnAlNO_3$–HT	$ZnAlSO_4$–HT
5	70.8	84.7	11.5	49.0
10	74.3	113.7	39.5	55.6
15	131.0	107.4	62.1	54.3
20	188.9	119.4	67.9	161.0

TABLE IV TG and DSC transformation temperatures of $ZnAlA^{n-}$–HT

Compounds	TG transformation temp. (°C)		Weight loss for T_1 (%)	DSC transformation temp. (°C)	
	T_1	T_2		T_1	T_2
$ZnAlCO_3$–HT	166	268	13.5	217	256
ZnAlCl–HT	128	253	12.6	173	236
	189	352			400
		556			
$ZnAlNO_3$–HT	100	219	7.5	175	240
		264			270
		404			440
$ZnAlSO_4$–HT	164	317	15.2	83	314
		(820)[a]		208	–

[a] Third weight loss.

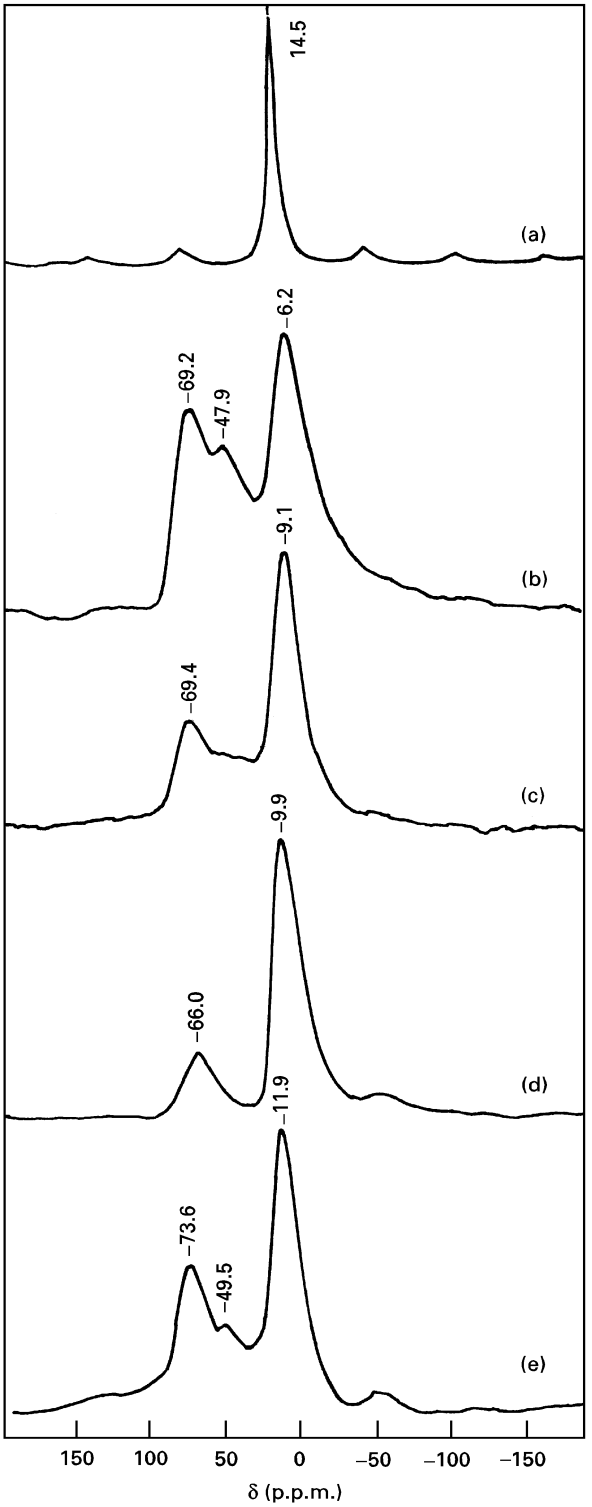

Figure 6 ^{27}Al MAS NMR spectra of (a) $ZnAlCO_3$–HT (uncalcined), (b) $ZnAlCO_3$–HT, (c) ZnAlCl–HT (d) $ZnAlNO_3$–HT (e) $ZnAlSO_4$–HT calcined at 500 °C for 4 h.

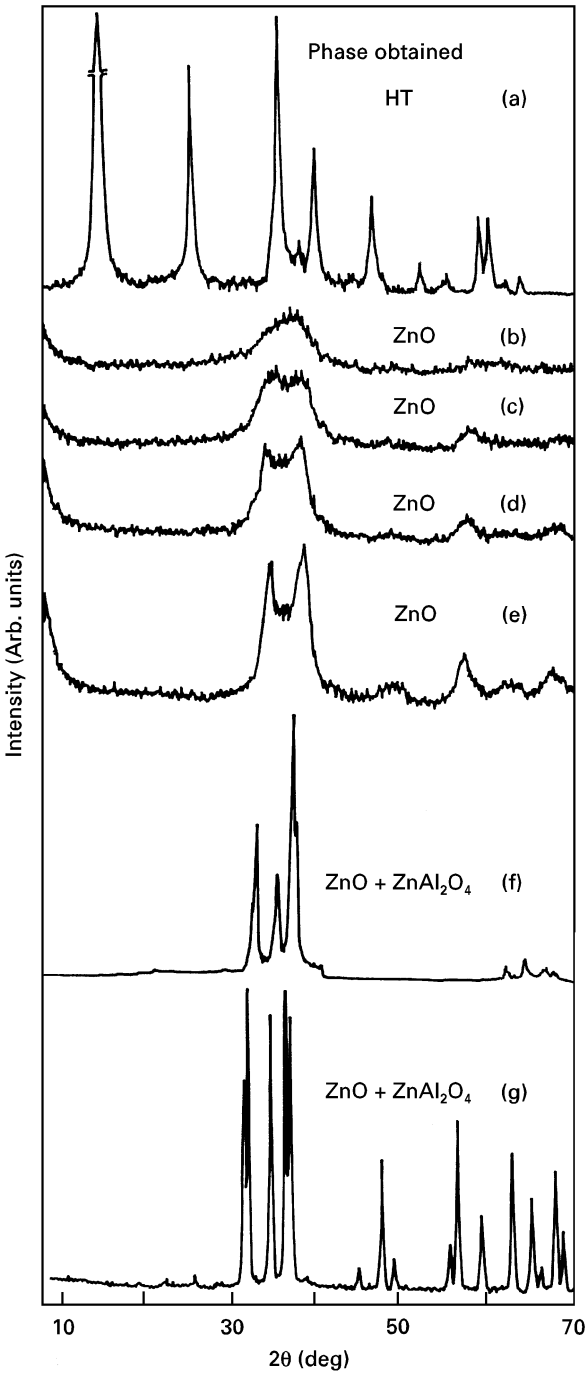

Figure 7 Powder X-ray diffraction patterns of $ZnAlCO_3$–HT calcined at (a) 150, (b) 200, (c) 300, (d) 400, (e) 600, (f) 800, (g) 1200 °C for 4 h.

decomposition of gibbsite ($Al(OH)_3$) [21] and it has never been observed during the thermal decomposition of hydrotalcites. Thevenot *et al.* [22] noticed a very weak resonance at 50 p.p.m. in the uncalcined ZnAl–HT with a Zn/Al atomic ratio of 3 and attributed it to Al^{IV}. Moreover, extensive ^{27}Al MAS NMR studies by several researchers [8, 21, 23] on the thermal decomposition of $MgAlCO_3$–HT have noticed only two resonance frequencies, one corresponding to Al^{VI} around 10 p.p.m. and the other corresponding to Al^{IV} around 70 p.p.m. The formation of Al^{V} only in the case of $ZnAlCO_3$–HT and $ZnAlSO_4$–HT is surprising, and at this moment a suitable explanation is not available. One plausible reason could be the decomposition of bridged bidendate complex of anions of the type CO_3^{2-} and SO_4^{2-} with metal ions in the brucite-like layer. Such a type of coordination may not be possible in the case of monovalent anions. The tailing of the Al^{V} with Al^{IV} in the case of ZnAlCl–HT may be due to the binuclear bridging ability of the Cl^- ion. Further work is necessary in order to confirm these assumptions.

The variation of PXRD patterns with calcination temperature for $ZnAlCO_3$–HT (Fig. 7) indicates that the HT structure survives up to 150 °C. At 250 °C, the

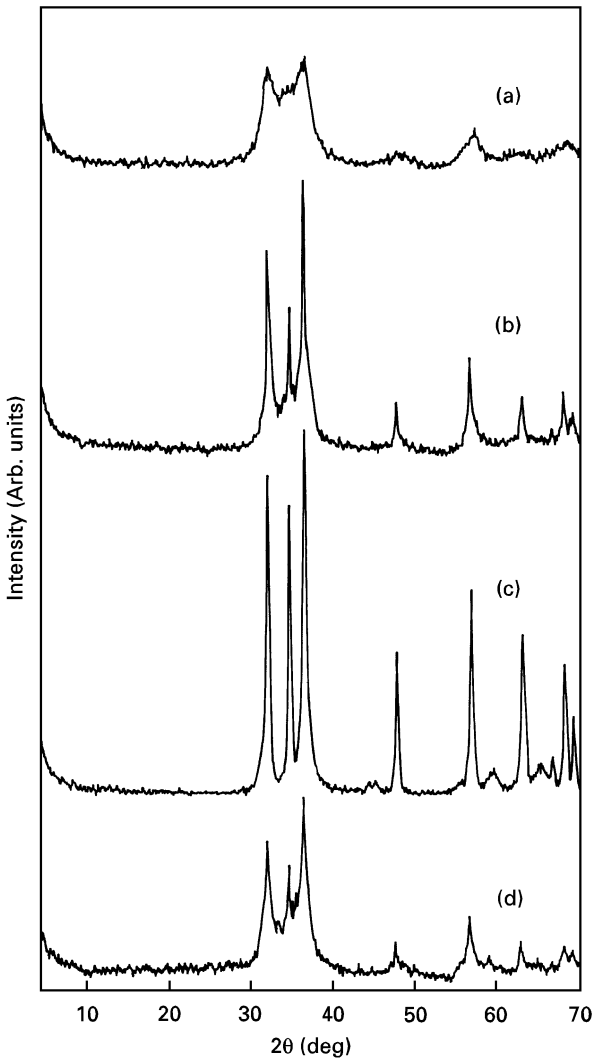

Figure 8 Powder X-ray diffraction patterns of (a) $ZnAlCO_3$–HT, (b) ZnAlCl–HT, (c) $ZnAlNO_3$–HT, (d) $ZnAlSO_4$–HT calcined at 500 °C for 4 h.

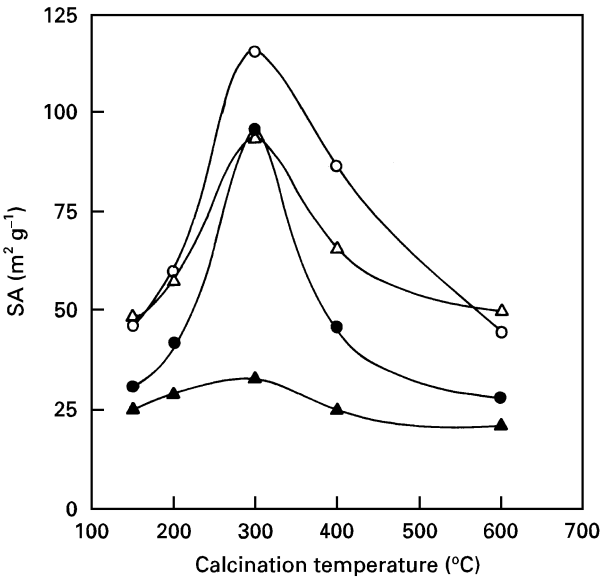

Figure 9 Variation of surface area with calcination temperature for $ZnAlA^{n-}$–HT. (○) $ZnAlCO_3$–HT, (△) ZnAlCl–HT, (●) $ZnAlNO_3$–HT, (▲) $ZnAlSO_4$–HT.

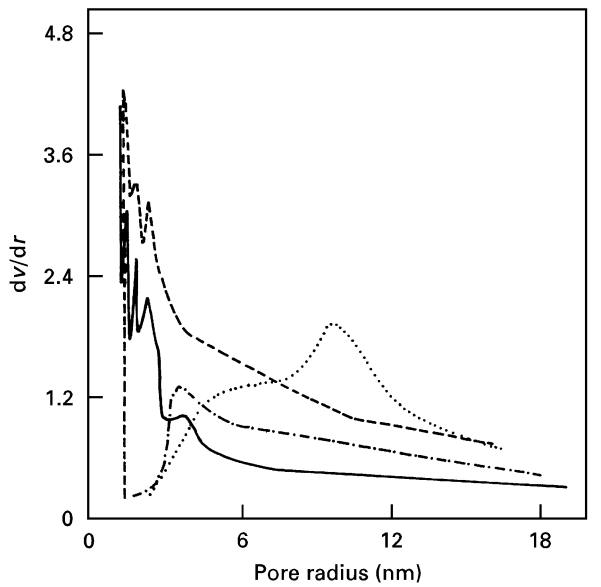

Figure 10 Pore-size distribution of $ZnAlA^{n-}$–HT calcined at 500 °C for 4 h. (——) $ZnAlCO_3$–CHT, (– – –) ZnAlCl–CHT, (· · ·) $ZnAlNO_3$–CHT, (—·—) $ZnAlSO_4$–CHT.

layer structure collapses and forms a highly amorphous ZnO phase whose crystallinity increases with increase in calcination temperature up to 600 °C. The thermally transformed products at 800 °C were ZnO and $ZnAl_2O_4$ spinel. Further calcination to 1200 °C improves the crystallinity of these two products. The PXRD pattern of all these samples calcined at 500 °C for 4 h (Fig. 8) shows that the product obtained in the decomposition reaction is a non-stoichiometric ZnO whose crystallinity depended on the nature of the interlayer anion. It is clear from Fig. 8, that the $ZnAlNO_3$–HT offered a well-crystalline ZnO compared to ZnAlCl–HT or $ZnAlSO_4$–HT. The $ZnAlCO_3$–HT yielded a poorly crystalline ZnO. The PXRD results are further supported by the variation of surface area with calcination temperature (Fig. 9) which showed a substantial decrease in surface area in the case of $ZnAlNO_3$–HT (from 96 $m^2 g^{-1}$ to 28 $m^2 g^{-1}$) compared to ZnAlCl–HT (from 94 $m^2 g^{-1}$ to 50 $m^2 g^{-1}$). The evolution of NO_2 and NO gases from $ZnAlNO_3$–HT during calcination (cf: EGA results) favours the formation of well-crystalline ZnO compared to other $ZnAlA^{n-}$–HT.

The pore-size distribution curves for all these samples calcined at 500 °C/4 h are shown in Fig. 10. It can be seen that $ZnAlCO_3$–HT and ZnAlCl–HT display a narrow pore-size distribution with a pore radius of around 1.5 nm indicating that the micropores contribute to the total surface area. On the other hand, a broad distribution of pores is noticed with a maximum centred around 10 nm for $ZnAlNO_3$–HT and around 4 nm for $ZnAlSO_4$–HT demonstrating the contribution of mesopores to the total surface area of these samples.

The lattice parameters calculated for ZnO (hexagonal) obtained from the calcination of $ZnAlA^{n-}$–HT considering (1 0 1), (1 0 0) and (0 0 2) planes (Table V) showed that, the calculated a_0 values are less than the actual value indicating the dissolution of aluminium in the ZnO lattice. The difference in a_0 value among the calcined samples reveals that the extent of solid

TABLE V Lattice parameters of ZnAlA^{n-}–HT calcined at 500 °C for 4 h

Compounds	Lattice parameters	
	a_0 (nm)	c_0 (nm)
$ZnAlCO_3$–HT	0.3174	0.5184
ZnAlCl–HT	0.3190	0.5184
$ZnAlNO_3$–HT	0.3236	0.5184
$ZnAlSO_4$–HT	0.3281	0.5256
ZnO[a]	0.3249	0.5205
$ZnAl_2O_4$[b]	0.8085	–

[a] JCPDS file number 5.0664.
[b]JCPDS file number 5.0669.

solubility decreases in the order $ZnAlCO_3$–CHT > ZnAlCl–CHT > $ZnAlNO_3$–CHT. This order seems to be the reverse of the crystallinity of these products (Fig. 8). The lattice parameter of ZnO in $ZnAlSO_4$–HT (0.3281 nm) is surprisingly higher in comparison with pure ZnO (0.3249 nm). This may be due to the formation amorphous $ZnSO_4$ phase present in addition to ZnO. Furthermore, in $ZnAlSO_4$–HT, there is no marked difference in the surface area (20–30 $m^2 g^{-1}$) with calcination temperatures (Fig. 9) which could be attributed to the adsorption of SO_4^{2-} ions on the thermally decomposed products. From these results it can be inferred that the structural and textural properties are affected by the presence of different anions in the interlayer of hydrotalcite-like compounds.

4. Conclusions

1. The nature of the interlayer anion plays a profound role in controlling the crystallinity and the textural properties of the fresh, as well as the calcined, samples.

2. Except for the NO_3^- ion, the symmetry of the other anions is reduced upon intercalation due to the interaction between the brucite-like layer and the anion. The nature of the anions also influences the ordering of the cation distribution, which follows the order $ZnAlCO_3$–HT > ZnAlCl–HT > $ZnAlNO_3$–HT > $ZnAlSO_4$–HT.

3. The activation energy for the decomposition of the brucite-like layer is in the order $ZnAlCO_3$–HT > $ZnAlSO_4$–HT > ZnAlCl–HT > $ZnAlNO_3$–HT.

4. Formation of pentacoordinated aluminium is noticed for the first time during the thermal decomposition of ZnAlA^{n-}–HT.

5. Calcination of these materials around 500 °C yields non-stoichiometric ZnO whose crystallinity seems to be the reverse of the solid solubility.

Acknowledgements

The authors thank Mrs Rama and Mr M. S. Moni for their expert technical assistance, RSIC IIT, Madras for ICPES, ^{27}Al MAS NMR and laser Raman spectra. S.V. thanks IIT, Madras, for the award of a research fellowship.

References

1. W. T. REICHLE, *J. Catal.* **94** (1985) 547.
2. S. VELU and C. S. SWAMY, *Appl. Catal* **119** (1994) 241, and references therein.
3. A. CORMA, S. IBORRA, J. PRIMO and F. REY, *ibid.* **114** (1994) 214.
4. M. J. CLIMENT, A. CORMA, S. IBORRA and J. PRIMO, *J. Catal.* **151** (1995) 60.
5. D. TICHIT, M. H. LHOUTY, A. GUIDA, B. H. CHICHE, F. FIGUERAS, A. AUROUX, D. BARTALINI and E. GARRONE, *ibid.* **151** (1995) 50.
6. V. R. L. CONSTANTINO and T. J. PINNAVAIA., *Catal. Lett.* **23** (1994) 361.
7. C. T. FISHEL, and R. J. DAVIS, *ibid.* **25** (1994) 87.
8. J. SHEN, J. M. KOBE, Y. CHEN and J. A. DUMESIC, *Langmuir* **10** (1994) 3902.
9. A. OOKUBO, K. OOI and H. HAYASHI, *ibid.* **9** (1993) 1418.
10. C. MOUSTY, S. THERIAS, C. FORNANO and J. BESSE, *J. Electroanal. Chem.* **374** (1994) 63.
11. J. WANG, Y. TIAN, R. WANG and A. CLEARFIELD, *Chem. Mater.* **4** (1992) 1276.
12. V. R. L. CONSTANTINO and T. J. PINNAVAIA, *Inorg. Chem.* **34** (1995) 883.
13. M. J. HERNANDEZ, M. A. ULIBARRI, J. I. RENDON and C. J. SERNA, *Thermochim. Acta* **81** (1984) 311.
14. S. MIYATA and A. OKADA, *Clays Clay Mineral.* **25** (1977) 14.
15. S. KANNAN, S. VELU, V. RAMKUMAR and C. S. SWAMY, *J. Mater. Sci.* **30** (1995) 1462.
16. S. KANNAN and C. S. SWAMY, *ibid.*, in press.
17. S. MIYATA, *Clays Clay Mineral.* **23** (1975) 369.
18. E. KANEZAKI, K. KINUGAWA and Y. ISHIKAWA, *Chem. Phys. Lett.* **226** (1994) 325.
19. T. SATO, S. ONAI, T. YOSHIOKA and A. OKUWAKI, *J. Chem. Tech. Biotechnol* **57** (1993) 137.
20. M. J. HERNANDEZ-MORENO, M. A. ULIBARRI, J. L. RENDON and C. J. SERNA, *Phys. Chem. Mineral.* **12** (1985) 34.
21. K. J. D. MACKENZIE, R. H. MEINHOLD, B. L. SHERRIFF and ZHIXU, *J. Mater. Chem.* **3** (1993) 1263.
22. F. THEVENOT, R. SZYMANSKI and P. CHAUMETTE, *Clays Clay Mineral.* **37** (1989) 396.
23. S. VELU, DOROTHY SAMUEL and C. S. SWAMY, in "Catalysis: Modern Trends", edited by N. M. Gupta and D. K. Chakrabarthy (Narosa, New Delhi, India, 1995) p. 470.

Received 16 February
and accepted 31 July 1996